Nano Research

ISSN 1998-0124 CN 11-5974/O4
https://doi.org/10.1007/s12274-021-3386-z

Flagship Review

Flexible organic solar cells for biomedical devices

Bin Kan[1], Faheem Ershad[2], Zhoulyu Rao[3], and Cunjiang Yu[1,2,3,4,5] (✉)

[1] *Department of Mechanical Engineering, University of Houston, Houston, TX 77204, USA*
[2] *Department of Biomedical Engineering, University of Houston, Houston, TX 77204, USA*
[3] *Materials Science and Engineering Program, University of Houston, Houston, TX 77204, USA*
[4] *Department of Electrical and Computer Engineering, University of Houston, Houston, TX 77204, USA*
[5] *Texas Center for Superconductivity, University of Houston, Houston, TX 77204, USA*

Received: 23 December 2020 / **Revised:** 15 February 2021 / **Accepted:** 18 February 2021

ABSTRACT

Organic solar cells (OSCs), particularly made based on solution processing methods, have made significant progress over the past decades through the concurrent evolution of organic photovoltaic materials and device engineering. Recently, high power conversion efficiencies around 18% and over 16% have been demonstrated in both rigid and flexible OSCs, respectively. While most of the OSC research has centered on efficiency and cost, their emerging and potential usages in many critical applications, particularly in biomedical fields have been rising. In this mini-review, we will briefly discuss the high-performance organic photovoltaic materials and the representative flexible OSCs to give a scope on the recent rapid development of OSCs. Besides, we will review some progress on the applications of OSCs in biomedical devices and integrated systems. The potential challenges associated with integrating OSCs for biomedical devices will be put forward.

KEYWORDS

organic solar cells, photovoltaic, flexible, biomedical, bioelectronics

1 Introduction

Organic solar cells (OSCs), particularly made based on solution processing methods, which possess the advantages of scalable manufacturing, low-cost, lightweight, and mechanical flexibility, are regarded as one of the promising technologies to convert solar energy into electricity [1]. The state-of-the-art OSC device usually has a sandwich configuration, in which the active layer materials are layered between two electrodes with different work functions. Thanks to the invention of the bulk-heterojunction structure with interpenetrating donor/acceptor (D/A) networks, efficient charge generation and separation can occur in the active layer with a thickness of ~ 100 nm [2, 3]. For the past three decades, concerted efforts have been made by chemists, physicists, and engineers to develop novel materials, understand the photophysical mechanism, optimize the nanoscale phase separations, and improve the OSC performances [4–8]. In terms of their power conversion efficiencies (PCEs), over 18% for single-junction OSCs [9–11] and over 17% for tandem OSCs [12] have been successfully demonstrated. Such high PCEs cannot be achieved without the help of polymer donor materials and acceptor-donor-acceptor (A-D-A) structured nonfullerene acceptors (NFAs) [13–16]. As a matter of fact, the distinctive NFAs not only avoid some limitations of typical fullerene acceptors but also open a new pathway to increase the overall performance [8, 17, 18]. Theoretical predictions suggest that PCEs over 20% for single-junction OSCs and over 25% for tandem OSCs can be achievable by molecular optimizations and device engineering, encouraging the community towards further exploration [12, 19].

Nowadays, the highest OSC performances are mostly obtained by the indium tin oxide (ITO)-based rigid devices with small effective areas. Besides these, flexible devices with ultra-thin structures display comparable performances with their rigid counterparts. One of the key components of a flexible device is the flexible transport electrode (FTE). Several effective strategies have been implemented to fabricate the FTEs, such as sputtering ITO on the flexible polymer substrate (PET or PEN), and developing silver nanowires (AgNWs) or poly(3,4-ethylenedioxythiophene):poly(styrene sulfonate) (PEDOT: PSS) based transparent electrodes [20, 21]. For example, Chen's group developed FTEs using silver nanowires and a polyelectrolyte on a PET substrate [22]. The corresponding flexible device not only achieved a record PCE of 16.5%, but also exhibited long-term storage stability and robust mechanical stability. Along with the nascent novel wide-bandgap polymer donors and Y6 acceptor, high PCEs around 15% have been demonstrated for single-layer flexible devices [23–26]. All these devices can maintain their performances with multiple bending tests. These results indicate the potential of flexible OSCs in future portable and wearable applications, such as clothing and wristwatches.

As one of the photoelectric conversion technologies, OSCs have been utilized for many applications, ranging from energy systems (lithium battery and supercapacitor) [27–30], water splitting systems [31–33], and biomedical devices [34–36]. In particular, biomedical devices play a vital role in future healthcare by providing functions such as monitoring the health of the human body and providing therapeutic functions [37–43]. For instance, Someya's group reported self-powered ultra-flexible

Address correspondence to cyu15@uh.edu

electronics for biomedical devices, in which the flexible OSC device was integrated with an organic electrochemical transistor to measure biometric signals with high signal-to-noise ratios (SNR) when attached to the skin or other tissues [44]. Moreover, the long-term stability and relatively high-power output ability are both beneficial for biometric signal recording. Employing a high-performance flexible OSC device as the power source for bioelectronics encourages the development of future self-powered and bio-integrated electronics and systems.

This mini-review mainly focuses on flexible OSCs for biomedical applications. We will start with an introduction of high-performance organic photovoltaic materials to give the reader a broad scope on the recent rapid development of OSCs. Secondly, to meet the demand of bioelectrical applications, the flexible OSCs with representative results will be discussed. Then, the applications of OSCs in bioelectronics will be summarized. Lastly, we will put forward the challenges and future of integrated devices with OSCs and bioelectronics.

2 High-performance organic photovoltaic materials

The active layer of OSCs usually consists of electron donor and acceptor materials with suitable energy levels and balanced charge transport abilities. Note that the absorption ranges of the active layer are the prerequisites for efficient conversion of photons and thus, determining the current output [45, 46]. Generally, organic photovoltaic materials play a decisive role in enhancing their performance [5, 17, 47]. Polymer donor poly(alkyl thiophene) (such as P3HT) and fullerene acceptors dominated this research area in its early stage [48, 49]. However, their limited absorptions and unsatisfactory energy levels gave short-circuit current densities (J_{sc}) of ~ 10 mA·cm^{-2} and open-circuit voltages (V_{oc}) of 0.6 V, and thus PCEs around 3%–5%. Subsequently, developing donor-acceptor (D-A) featured polymer donors (such as PTB7 families) by narrowing the optical bandgap pushed PCEs to ~ 10% [50, 51]. Meanwhile, small-molecule donors with acceptor-donor-acceptor (A-D-A) backbones (such as DRCN5T) [52, 53] or donor-acceptor-donor-acceptor-donor (D_1-A-D_2-A-D_1) backbones (such as p-DTS(FBTTh$_2$)$_2$) [54] yielded PCEs around 10% when blended with a PCBM acceptor. Further device optimization with a ternary strategy or tandem device structure led to over 12% PCEs for fullerene-based devices [55, 56]. Since there is extensive literature on the history and development of fullerene-based devices, they will not be discussed here, and the reader is encouraged to browse the literature.

However, the intrinsic drawbacks of PCBM acceptors, such as weak absorption ability mainly in the visible range and weak chemical and electronic tunability, limit the further development of OSCs. To resolve these issues, NFAs with versatile chemical structures and properties have been developed over the past few years. Numerous NFAs based on perylene diimide (PDI), naphthalene diimide (NDI), large-fused ring units (such as IDTT, IDT and et al.), and other aromatic ring units have shown advantageous efficiencies and stabilities [14, 19, 57]. From their chemical structures and molecular weights, the organic photovoltaic materials can be classified into two classes: polymer and small-molecule materials. With these in mind, we will briefly discuss the recent development of NFA- based devices from four aspects in this section.

2.1 Polymer donor/small-molecule acceptor

Currently, the highest efficiency of OSCs was realized by combining wide bandgap polymer donors (PM6, D18) and low bandgap small-molecule acceptors (Y6 and its analogs) [47, 58]. The polymer donor/small-molecule acceptor (P_D/S_A) has the advantage of high film quality of polymer materials and easily-tunable properties of both materials. Among different types of acceptors, S_A materials with A-D-A architecture have drawn much interest because of their defined structures and simple tunability [14, 19]. In 2015, Zhan et al. reported a typical A-D-A acceptor ITIC based on the large fused-ring central core (IDTT) capped with two strong electron-withdrawing units (INCN) [59]. Its strong absorption ability in the infrared range and good electron mobility contributed to a promising PCE of 6.80% when blended with the polymer donor PTB7-Th. The A-D-A structured NFAs provide several advantages: 1) the energy levels can be precisely modified by tuning the chemical structures of the central fused-ring unit and/or the ending units; 2) strong intramolecular charge transfer (ICT) process between central D and ending A units leads to efficient absorption extending to the near infrared range; 3) multiple side-chains enable their good solubility in common organic solvents and prevent excessive self-aggregation in the nanoscale morphology.

Inspired by these aspects, studies have shown that modifying the D, A, and side-chains produced a vast amount of S_A materials with various bandgaps ranging from 1.80–1.20 eV, and different molecular packing and charge transport properties [13, 14, 60]. Meanwhile, developing wide bandgap donors to provide a complementary absorption with these acceptors is quite important to convert as many of the photons as possible [61, 62]. Hou et al. reported the devices based on a wide-bandgap polymer donor PBDB-T and acceptor ITIC, which offered a broader absorption range from 400–800 nm and well-aligned energy levels [63]. The devices displayed a PCE over 11% with both high J_{sc} and V_{oc}. The concurrent evolution of wide bandgap polymers and small-molecule acceptors significantly improved the PCEs to 12%–15% for single-layer OSCs. For example, the combination of the fluorinated polymer donor PM6 and the fluorinated acceptor IT-4F delivered a PCE of 13.5% [64, 65]. The halogen-substituted strategy in donor and acceptor materials represents one of the most successful and widely-used methods of designing high-performance organic photovoltaic materials.

In 2019, Zou et al. reported a new acceptor Y6 based on a multi-fused ring central unit with electron-deficient benzothiadiazole core (TPBT) (Fig. 1) [66]. The synergistic contribution of the TPBT core and fluorinated ending groups help to enable an efficient absorption ability extending to 950 nm and maintain its suitable lowest unoccupied molecular orbital (LUMO)/highest occupied molecular orbital (HOMO) energy levels to match the wide-bandgap donors with a low-lying HOMO level. A PCE over 15% was recorded in its first implementation in OSCs by pairing with PM6. Recently, by fine-tuning the chemical structure of TPBT and device optimization, high efficiencies over 18% have been realized [10, 67]. The invention of Y6 families makes it possible to achieve ~ 20% PCEs for the devices using polymer donors and small-molecule acceptors [58, 68].

2.2 Small-molecule donor/small-molecule acceptor

Small-molecule materials have well-defined chemical structures and thus less batch-to-batch variation, easily-tunable properties, and purification process [69–71]. Thus, constructing OSCs with small-molecule donors and small-molecule acceptors (S_D/S_A) can fully exploit these advantages. However, due to the similar chemical structures and usually strong crystalline behavior of small molecules, the corresponding active layers sometimes exhibit homogeneous morphologies without suitable nanoscale phase separation, or large-scale phase separation and crystalline domains in blends. These factors lead to the

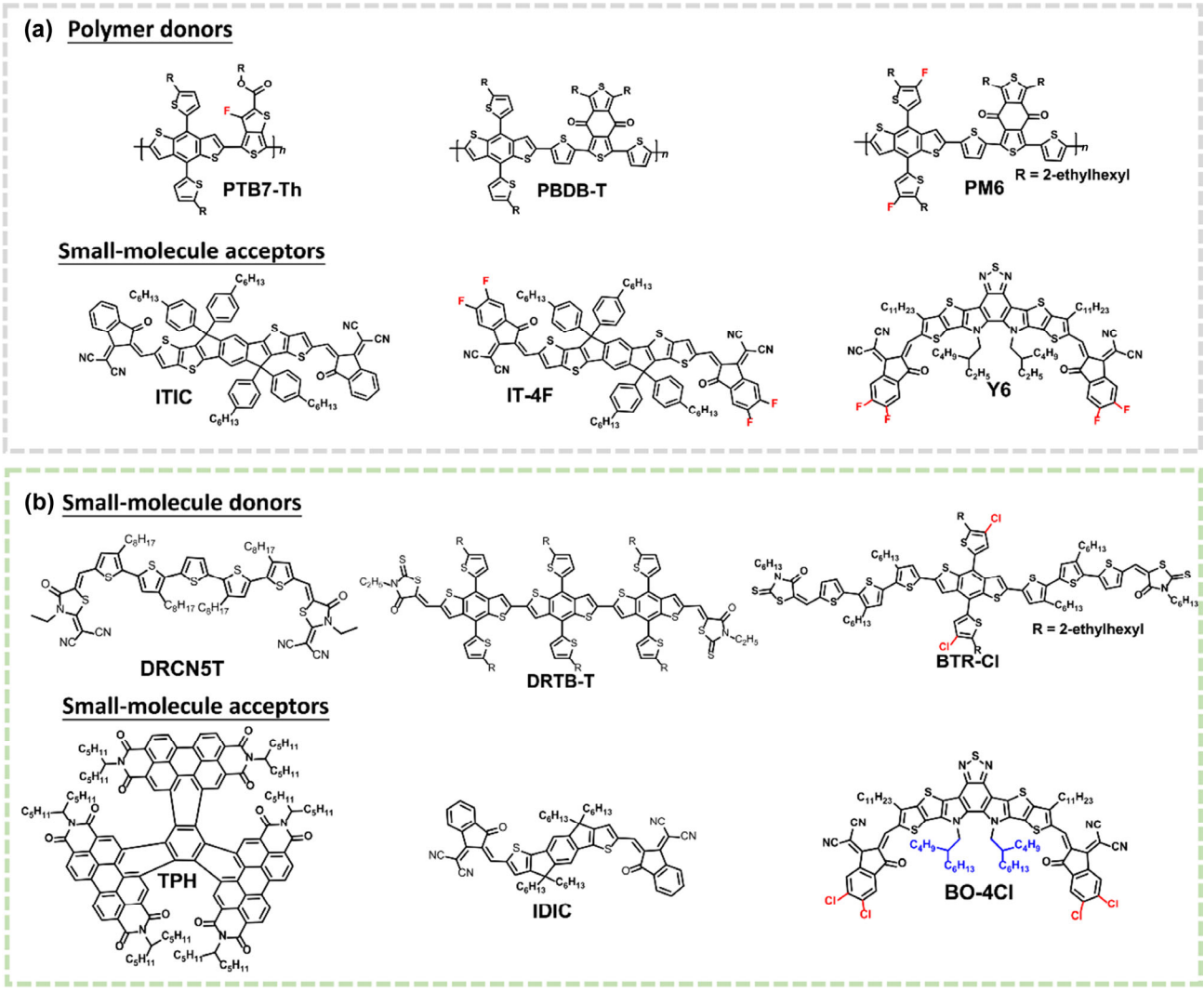

Figure 1 (a) Chemical structures of polymer donors (PTB7-Th, PBDB-T and PM6, respectively) and small-molecule acceptors (ITIC, IT-4F and Y6, respectively). (b) Chemical structures of small-molecule donors (DRCN5T, DRTB-T and BTR-Cl, respectively) and chemical structures of small-molecule acceptors (TPH, IDIC and BO-4Cl, respectively).

challenges of S_D/S_A based devices, which have only displayed efficiencies around 3%–7% prior to 2017, and are even inferior to those of their fullerene-based counterparts [72]. For example, a device based on DRCN5T:TPH exhibited a PCE of 6.16%, which is much lower than that of a DRCN5T: $PC_{71}BM$ based device (PCE of 10.10%) [73].

An alkylated acceptor IDIC with enhanced electron mobility of 1.1×10^{-3} $cm^2 \cdot V^{-1} \cdot s^{-1}$ and strong crystallinity was employed in the fabrication of all-small-molecule-based devices [74]. The first report using the acceptor IDIC and donor DRTB-T gave a promising PCE over 9% due to their complementary absorptions and optimized morphologies [75]. Solvent vapor annealing (SVA) and thermal annealing (TA) treatment were adopted to control their morphologies which featured domain sizes on the order of tens of nanometers. With continuous optimization of S_D materials, the IDIC acceptor based all-small molecule devices yielded over 11% PCEs, which are comparable to those of the fullerene-based devices [76, 77]. In addition, plenty of alkylated S_A materials based on different large-fused ring cores and ending units have been rationally designed and reported to pair with S_D materials. For example, the DRCN5T based all-small molecule devices achieved nearly 10% efficiency when F-2Cl was developed as a new acceptor [78]. Recently, Lu et al. employed the liquid crystalline small-molecule donor BTR to pair with the acceptor Y6 [79]. With chlorinated side-chains and further device optimization, a high efficiency of 15.34% was obtained for the BTR-Cl:Y6:$PC_{71}BM$ based ternary devices [23]. Meanwhile, Hou et al. achieved a certified result with 15.1% efficiency by precisely controlling the structures of the small-molecule donor (B1) and acceptor (BO-4Cl)[80]. These results suggest the importance of developing S_D and S_A materials simultaneously.

2.3 Polymer donor/polymer acceptor

Apart from the S_A materials, polymer acceptor (P_A) materials have received increased attention due to their distinct merits of superior thermal stability and enhanced mechanical properties [81, 82]. The P_D/P_A based devices have continuously improved with recent reports showing encouraging PCEs over 14% [60]. The polymer acceptor N2200 based on NDI and a thiophene unit, which was first reported in 2009, yields a high electron mobility of 0.06 $cm^2 \cdot V^{-1} \cdot s^{-1}$ and two obvious absorption peaks located at visible and infrared ranges [83]. Though the first case of P_D/P_A using N2200 resulted in a poor performance of 0.16% [84], synergistically modifying the backbones of N2200 and P_D contributed to higher efficiencies of 8%–10% [85, 86]. For example, the combination of polymer donor J51 and N2200 displays well-matched absorption ranges and electronic energy levels, which helped to obtain a J_{sc} of 14.18 $mA \cdot cm^{-2}$, a V_{oc} of 0.83 V, and thus, a good PCE of 8.27% [87].

Besides the D-A type copolymer acceptors, Li et al. demonstrated a creative strategy to synthesize the polymer acceptor PZ1, in which the A-D-A type monomer was embedded into the polymer chain [88]. The features of the A-D-A monomer, such as its coplanar structure, high electron affinity, and good absorption ability, can be well maintained in the corresponding polymers. Furthermore, the good film quality, additional electron-transporting channels through the polymer chains, and tunable photophysical properties of this novel P_A are beneficial for obtaining high-performance all-polymer devices. As a result, PZ1 displays a low optical bandgap of 1.55 eV and a high absorption coefficient. The corresponding devices based on PBDB-T:PZ1 achieved a top PCE of 9.19% in 2017. Later studies showed that changing the linker unit or modifying the large fused-ring unit resulted in several PZ1 analogs with improved performance, and these results suggested a successful and effective strategy by embedding the A-D-A monomer into the design of P_A materials.

Recently, the backbone of the Y6 acceptor was also demonstrated in P_A materials by adopting the same method. The long branch alkyl chains enable the good solubility of the resulting polymers. The polymer acceptor PJ1, which consists of the Y6 backbone and the thiophene linker, has a narrow bandgap of 1.40 eV and good electron transport property [60]. An all-polymer OSC using PBDB-T:PJ1 obtained a maximum PCE of 14.4% with low energy loss. More importantly, the device exhibited a quite stable morphology with high efficiency retention ratio under thermal annealing. The combination of PM6 and PJ1 analogues (PYT1) achieved a similar high PCE of 13.43% with an energy loss below 0.50 eV [89]. By further optimizing their structures, P_D/P_A devices have great potential in achieving high PCEs and outstanding thermal and mechanical stability.

2.4 Small-molecule donor/polymer acceptor

Liu et al. demonstrated efficient and thermally stable OSCs based on S_D/P_A blends, in which the S_D is DR3TBDTC and the P_A is PBN-11 (Fig. 2) [90]. Unlike traditional S_D materials with strong crystallinity, DR3TBDTC shows suppressed-stacking behaviors due to the large steric hindrance effect of side-chains. Hence, suitable phase separations can be observed in the S_D/P_A active layer, which further led to a promising efficiency of 8.0%. This S_D/P_A combination also displayed very impressive thermal stability under a high temperature for 7 days. These results are expected to expand the research field of OSCs.

In this section, we discussed the development of high-performance organic photovoltaic materials. Apart from these, the morphologies of the active layers with interpenetrating D/A networks on the order of tens of nanometers are also vital for realizing high efficiency. Adding a third or fourth component to the above D/A blends can effectively tune the morphology and regulate their energy alignments, and thus improve the overall performance. These organic photovoltaic materials on the ITO-based rigid substrate are the key components for achieving high-performance flexible devices. Further developing narrow bandgap materials with excellent charge transportability and stability is still of importance and necessity.

3 Flexible organic solar cells

Flexible OSCs that are bendable, stretchable, and more lightweight have received tremendous attention due to their potential in wearable and biomedical devices [35, 44]. Nowadays, high-performance photovoltaic materials with over 18% PCEs provide

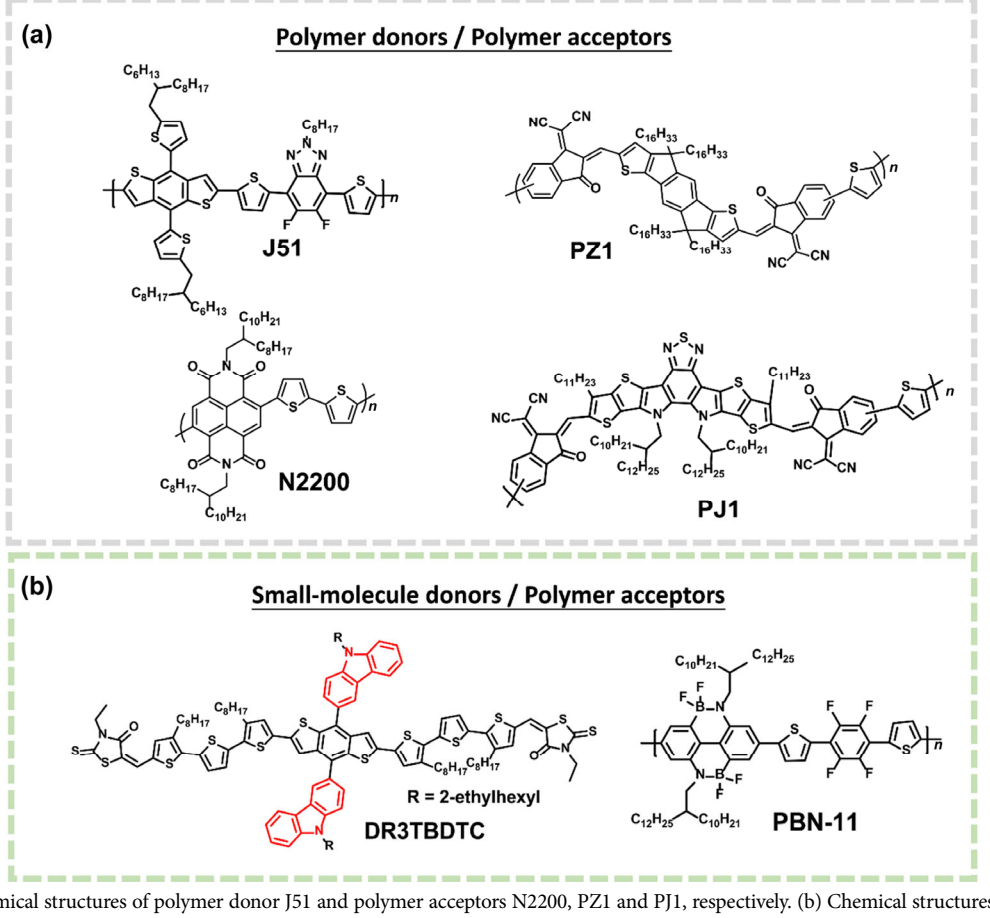

Figure 2 (a) Chemical structures of polymer donor J51 and polymer acceptors N2200, PZ1 and PJ1, respectively. (b) Chemical structures of small-molecule donor DR3TBDTC and polymer acceptor PBN-11, respectively.

a platform for realizing efficient flexible devices. The main challenge of flexible devices is the development of flexible transparent electrodes (FTE), which should have the characteristics of superior transparency, high conductivity, suitable work function, smooth surface, and excellent mechanical flexibility [21, 91–94]. Generally, the polymer flexible substrates, such as polyethylene terephthalate (PET), polyethylene naphthalate (PEN), and polyimide (PI), are indispensable. The active layers can be directly deposited on the FTE to fabricate the flexible devices. Since the development of fullerene based OSCs, developing FTEs has always been one of the important topics in the OSC field, and plenty of reports demonstrated various FTEs using ITO or ITO-free conductive materials.

3.1 Transparent ITO electrode based flexible devices

The ITO electrode is a widely used transparent conductive electrode in organic electronics, especially for solar cells. ITO-based rigid and flexible electrodes equipped with high conductivity and transparency are both commercially available nowadays. The devices on the rigid and flexible ITO-patterns can follow the same fabrication process, which usually display comparable PCEs. Zhou et al. achieved a maximum efficiency of 13.2% based on the active layer of PTB7-Th:IEICO-4F by optimizing the interfacial layer on the rigid ITO patterns [95]. After replacing the rigid substrate with a flexible one, no obvious decrease in performance was observed for the corresponding flexible solar cell, which showed a high PCE of 12.5% (Figs. 3(a)–3(c)). The device displayed good mechanical flexibility and maintained 90% of the initial efficiency after 2,000 bending cycles with a bending radius of 5 mm ((Fig. 3(d)).

The polymer substrates (such as PET) of the commercial flexible ITO patterns usually have thicknesses greater than hundreds of micrometers. Someya's group developed ultra-thin FTEs by sputtering a 100-nm-thick ITO layer on a 1-μm-thick parylene substrate [96]. By combining stable active layers and implementing an inverted architecture, mechanically stable flexible OSCs with a total thickness of 3 μm were achieved, and the flexible device exhibited a PCE of 7.9% (Fig. 3(e)). The ultra-thin characteristic is quite beneficial for electronic textile applications. Furthermore, the devices were sandwiched with two elastomers to improve the water stability while maintaining its flexibility. The encapsulated devices showed superior water stability without sacrificing efficiency and mechanical property. This strategy can also be applied for ultra-thin PI substrates, as shown in Fig. 3(f). The flexible devices based on PTB7-Th:PCBM produced a PCE up to 10%, which is comparable to those of their rigid counterparts [97]. Importantly, the usage of a thermally stable PI substrate and teflon/parylene double-barrier layers enabled long-term device stability and ultra-thin characteristics with high mechanical compliance. These ultra-thin flexible OSCs with excellent stability can emerge as textile-compatible power generation devices for wearables, electronic textiles, and other sensors in the future. In addition, it is supposed that the output power ability of such types of devices can be significantly improved by adopting high-performance organic photovoltaic materials, such as PM6:Y6 blends which provide a complementary and broad absorption range extending to 950 nm, well-aligned energy level, and balanced charge transport property, and thus producing a high J_{sc}, V_{oc}, and fill factor (FF), simultaneously [66].

3.2 ITO-free based flexible devices

Despite these achievements associated with ITO-based flexible devices, the high-cost and intrinsic brittle property of

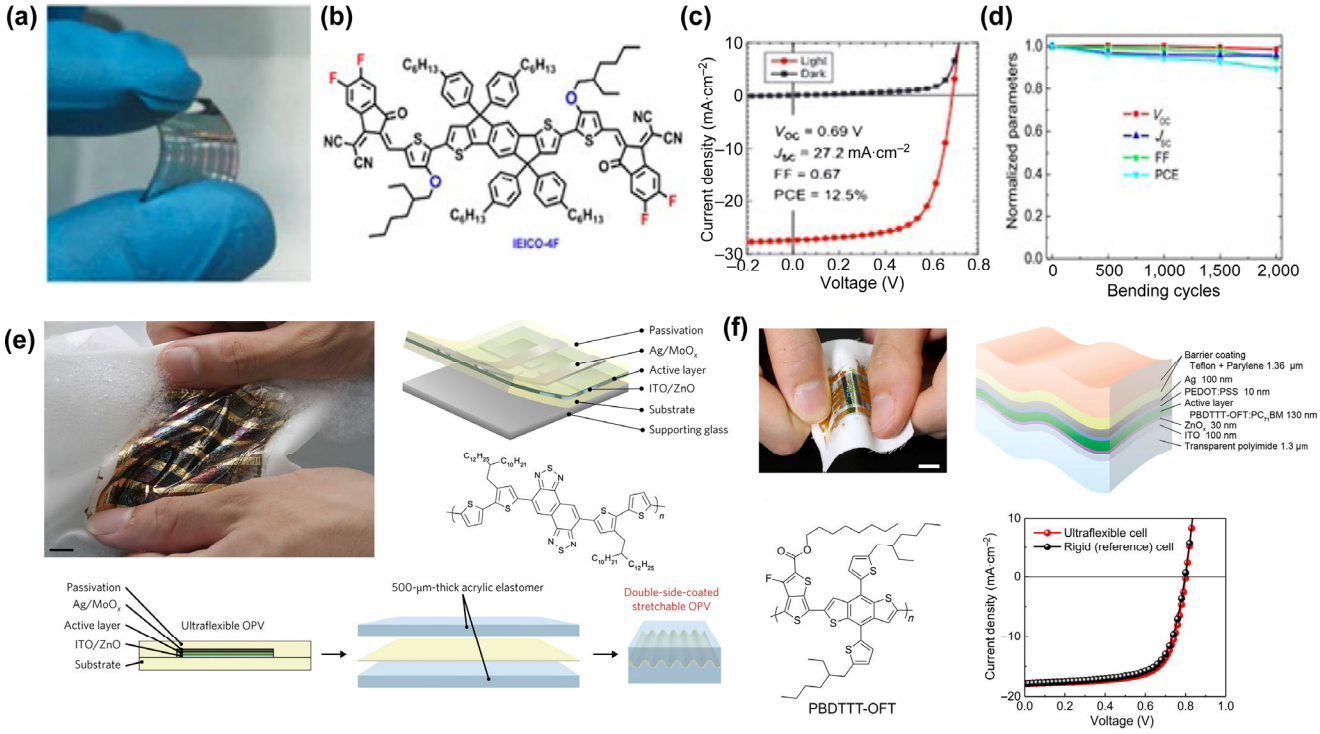

Figure 3 Flexible OSCs on the ITO based FTEs. (a) The illustration of a flexible OSC on the commercial ITO based FTE. (b) Chemical structure of IEICO-4F. (c) *J*–*V* curve of the flexible device using PTB7-Th:IEICO-4F. (d) Normalized device parameters of the PTB7-Th:IEICO-4F-based flexible solar cell as a function of bending cycles with a bending radius of 5 mm. (a)–(d) Reproduced with permission from Ref. [95], © WILEY-VCH Verlag GmbH & Co. KGaA, Weinheim 2019. (e) Washable ultra-thin flexible OSCs using ITO based FTEs, and structure of the free-standing OSCs, chemical structure of PNTz4T, and schematic of the double-side-coated OSCs. Reproduced with permission from Ref. [96], © Macmillan Publishers Limited, part of Springer Nature 2017. (f) Photograph of 3-μm-thick OSCs adhered on textile and the schematic of the ultra-thin OSCs, and *J*–*V* curves of the rigid and the flexible device. Reproduced with permission from Ref. [97], © Xu X., et al. 2018.

ITO limit its large-scale applications in the future. Thus, it is necessary to replace ITO with other conductive materials to develop ITO-free and low-cost FTEs. Many alternative transparent electrodes, such as carbon materials-based electrodes, ultra-thin metals, and metal grids, have been well investigated [20, 21, 98–101]. Here, we will discuss the solution-processed FTEs using AgNWs and conductive polymers (mainly PEDOT:PSS), which possess excellent conductivity and robust mechanical properties. It should be noted that nowadays, these two FTEs are widely used in the nonfullerene based OSCs with high performances.

Silver nanowires (AgNWs). AgNWs, which can be solution-processed, have been widely used to fabricate FTEs due to the excellent physical properties and conductivity of silver. The AgNWs were first used as the transparent electrode for OSCs in 2008 [102]. Compared to the ITO electrode, the AgNWs electrode obtained a similar or greater optical transparency at the same sheet resistance (~ 15 $\Omega \cdot sq^{-1}$) (Fig. 4(a)), leading to a slightly enhanced photocurrent. Subsequently, You et al. first demonstrated a AgNWs/PET anode for flexible OSCs, which yielded a recoverable efficiency of 2.5% under large deformations (Fig. 4(c)) [103]. The low work function of the AgNWs/PEDOT:PSS and the non-ideal ohmic contact between the FTE and the active layer led to their unoptimized performances. Still, these pioneering results implied that AgNW was a promising candidate for FTEs. Since then, great effort has been devoted to developing universal AgNWs-based FTEs for OSCs from several aspects including, for example, improving the surface roughness and the adhesion to the flexible substrate, controlling the work-function of the corresponding electrodes, and avoiding the oxidation of silver [22, 24, 25].

Recently, the development of nonfullerene photovoltaic materials has boosted the overall performances of the devices utilizing AgNWs-based FTEs. With the guide of an empirical model, Chen et al. demonstrated a record efficiency of 17.3% for the tandem OSCs on the ITO rigid substrate [12]. Then,

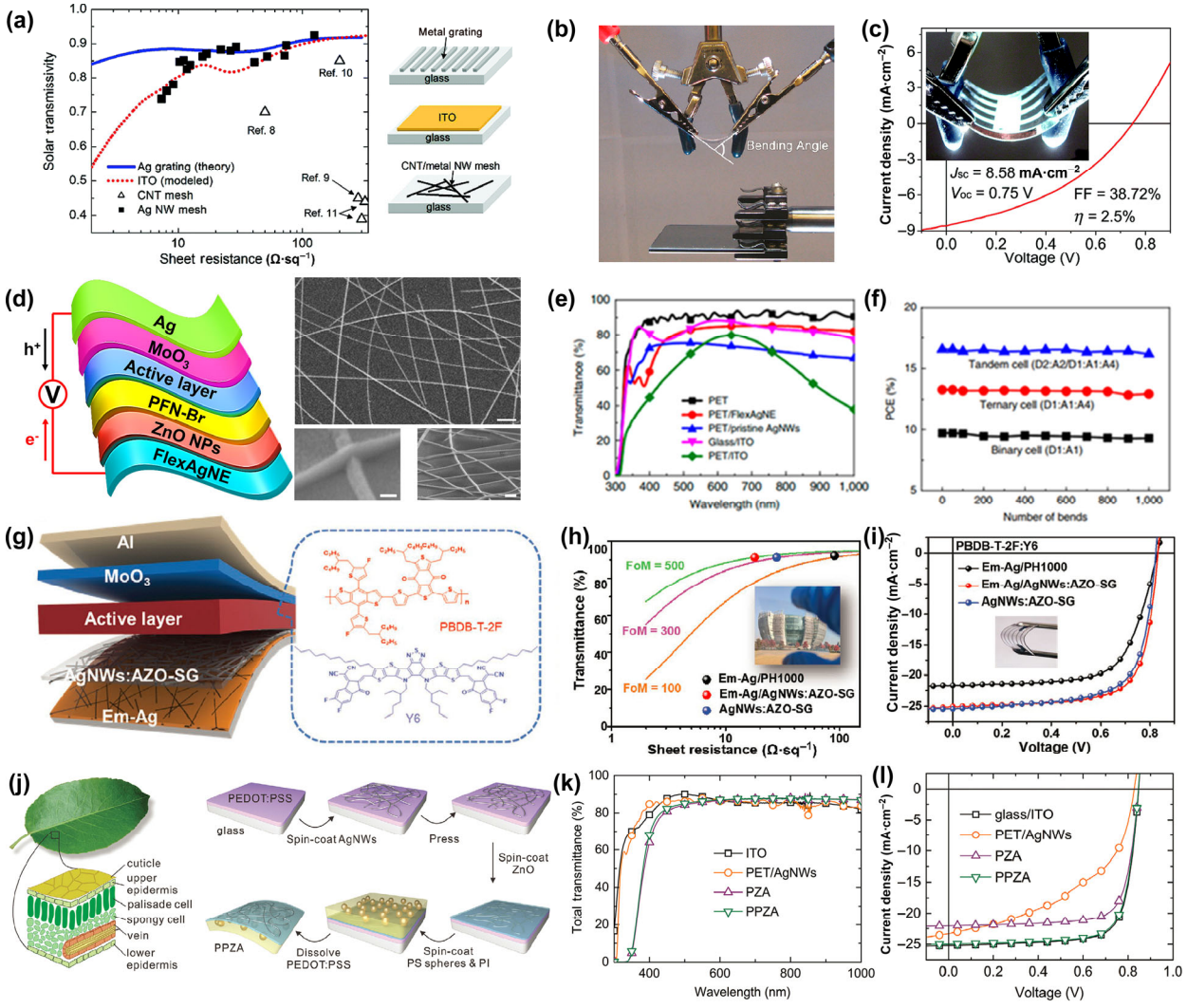

Figure 4 Flexible OSCs on the AgNWs based FTEs. (a) Solar photon transmissivity vs. sheet resistance for Ag gratings, ITO, CNT meshes and AgNW meshes deposited on the glass substrates. Reproduced with permission from Ref. [102], © American Chemical Society 2008. (b) and (c) The experimental setup used for measuring the *J*-*V* curves of flexible devices and the corresponding *J*-*V* curve of the device after bending, respectively. Reproduced with permission from Ref. [103], © American Chemical Society 2011. (d) The diagram of inverted flexible device reported by Chen et al. (e) Optical transmittance of the PET substrate, PET/FlexAgNE, PET/pristine AgNWs, glass/ITO, and PET/ITO. (f) PCE values for flexible devices as a function of the number of cycles of repeated bending at a bending radius of 5 mm. (d)-(f) Reproduced with permission from Ref. [22], © Sun Y., et al. under exclusive licence to Springer Nature Limited 2019. (g) Schematic illustration of a flexible OSC and chemical structures of the donor PBDB-T-2F and the acceptor Y6. (h) Transmittance of the flexible substrate (λ = 550 nm) plotted as a function of film sheet resistance. (i) *J*-*V* curves of the flexible devices. (g)-(i) Reproduced with permission from Ref. [25], © WILEY-VCH Verlag GmbH & Co. KGaA, Weinheim 2020. (j) Schematic of the fabrication of the biomimetic flexible electrode. (k) and (l) Transmission spectra of the various electrodes and *J*-*V* curves of the corresponding devices. (j)-(l) Reproduced with permission from Ref. [23], © WILEY-VCH Verlag GmbH & Co. KGaA, Weinheim 2020.

they successfully created an FTE using a water suspension of AgNWs and a negative-type PSSNa. Due to the ionic electrostatic charge repulsion, the resultant FTE has a smooth surface with low sheet resistance, high transparency of ~ 92%, and excellent mechanical flexibility. The FTE was used to fabricate the tandem devices, which gave a high PCE of 16.55%, representing the best result of flexible OSCs to date [22]. More importantly, the FTE can be successfully employed in fullerene and nonfullerene binary or ternary blends. As presented in Fig. 4(f), the performances of the different types of OSCs remained almost unchanged after bending 1,000 times with a bending radius of 5 mm, indicating the excellent mechanical stability of such flexible devices.

Li et al. adopted a welding strategy to develop FTEs with a tight binding of the upper electrode and the underlying PET substrate embedded with AgNWs (Fig. 4(g)) [25]. The upper hybrid electrode consists of solution-processed Al-doped zinc oxide and AgNWs network, which interact well with the AgNWs network of the underlying PET substrate. The integrated FTEs present a favorable sheet resistance, smooth surface, high optical transparency, and mechanical flexibility. Due to the outstanding photovoltaic properties of PM6:Y6, the corresponding flexible device displayed a high PCE of 15.21% with almost the same V_{oc}/J_{sc}/FF values in comparison with those obtained from the rigid ITO electrode-based devices. Besides, the flexible devices showed robust mechanical stability with 1,200 bending cycles at a radius of 4 mm, while retaining over 90% of their initial efficiencies. Recently, a record PCE of 16.1% was realized by a flexible OSC made with a biomimetic electrode design strategy inspired by the merits of a leaf [23]. As shown in Fig. 4(j), the biomimetic FTE was constructed by enveloping the AgNWs and the light scattering polystyrene (PS) spheres within a zinc oxide protecting layer on the flexible PI substrate. The newly designed FTEs simultaneously displayed a smooth surface, high transmittance around 90%, low sheet resistance, and excellent bendability. These advantages, together with the ternary blends of PM6:N3:$PC_{71}BM$, contributed to its outstanding PCE of 16.1%, which is comparable to the 16.2% of its corresponding rigid ITO-based device.

Nowadays, flexible OSCs based on the AgNWs FTE have shown their unique merits of high efficiency, robust mechanical flexibility, and universality for various organic photovoltaic materials. In the meantime, flexible devices with a large area of 1 cm^2 displayed over 12% PCEs, indicating the uniformity of the AgNWs based FTE. It is still necessary to improve the efficiency, enhance the long-term stability, and simplify the fabrication processes of AgNWs FTE in the future.

Conductive polymers (PEDOT:PSS). The most extensively investigated conductive polymer for constructing FTEs is PEDOT:PSS, which is composed of the conductive component PEDOT and the insulating component PSS [104–106]. Their chemical structures are presented in Fig. 5(a). Its work function and conductivity can be well manipulated by tuning the ratio of PEDOT to PSS. In a conventional OSC device, PEDOT:PSS

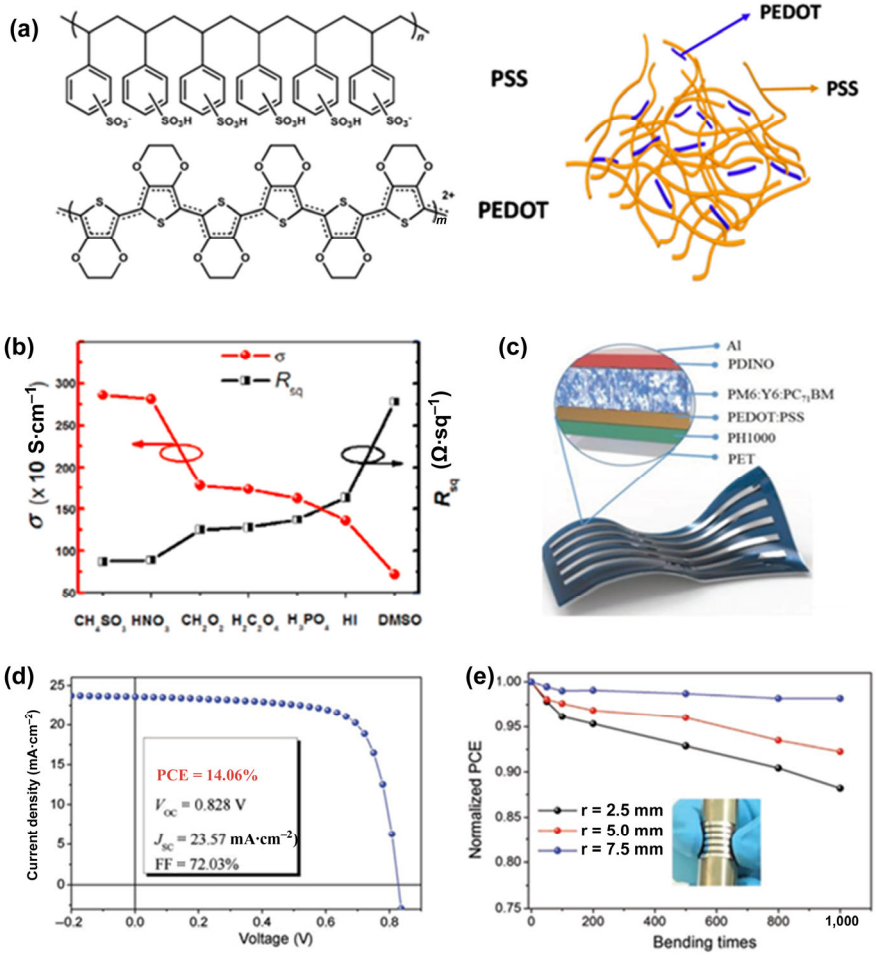

Figure 5 Flexible OSCs on the PEDOT:PSS based FTEs. (a) Chemical structures of PEDOT:PSS. (b) Comparison of square resistance and electrical conductivity of the PEDOT:PSS with diverse acid treatments at room-T and DMSO doping. Reproduced with permission from Ref. [109], © WILEY-VCH Verlag GmbH & Co. KGaA, Weinheim 2018. (c) The schematic structure of the flexible device. (d) *J*–*V* curve of the flexible device. (e) Bending performances with different bending diameters of the flexible devices. (c)–(e) Reproduced with permission from Ref. [110], © WILEY-VCH Verlag GmbH & Co. KGaA, Weinheim 2019.

(Clevios P VP AI 4083) is widely used as the hole transporting layer to modify the work function and the surface of ITO. Meanwhile, PEDOT:PSS with a lower ratio of PSS (such as PH1000) and thus enhanced conductivity can be used as a conductive transparent electrode [107, 108]. During the development of fullerene acceptors based OSCs, extensive efforts have been made to fabricate the PEDOT:PSS based FTEs, which should have high conductivity, low sheet resistance, and excellent optical transmittance.

Among different methods of treatment, organic acids, such as H_2SO_4, HNO_3, have been used to treat the pristine PEDOT:PSS films and tune the conductivity and sheet resistance (Fig. 5(b)). With systematic investigations, Ge et al. selected methanesulfonic acid (CH_3SOOH) to treat the PEDOT:PSS films on the flexible PET substrate at room temperature [109]. The slightly acidic property of CH_3SOOH not only prevents damage to the PET substrate but also enables a suitable work function of –4.91 eV for PEDOT:PSS films. Meanwhile, low sheet resistance and high conductivity were realized for the treated films. All these factors contributed to a high PCE of 14.06% for the flexible device based on a ternary blend of PM6:Y6:$PC_{71}BM$, which is the best result for PEDOT:PSS-based flexible OSCs to date [110]. The corresponding flexible device also displayed superior mechanical flexibility, which is supported by the high retention of the initial efficiency after 1,000 bending cycles under a radius of 7.5 mm. However, the performance of the flexible device was lower than the 16.67% PCE obtained with the rigid devices, mainly due to its relatively lower J_{sc} and FF. These results suggest that there is still much needed development to create efficient and stable FTEs based on PEDOT:PSS. It should be noted that the hygroscopicity and acidity of PEDOT:PSS are not advantageous for the long-term stability of the devices [110–112].

The aforementioned two conductive materials (AgNWs and PEDOT:PSS) have also been successfully utilized in the construction of ultra-thin flexible devices, recently [24]. As shown in Fig. 6(a), the transparent electrodes were deposited on 1.3 μm polyethylene naphthalate (PEN) substrates, which is the key factor to produce ultra-thin flexible devices with a total thickness of 2 μm. The newly-developed low work function interlayer of zinc ion chelated polyethylenimine (PEI-Zn) plays a vital role in matching the promising nonfullerene active layers. As a result, the ultra-thin flexible devices using PBDB-T-2F:Y6 binary blend achieved a PCE of 12.3% and 15.0% on PEDOT:PSS and AgNWs electrodes, respectively. When the resultant devices were attached on a pre-strained elastomer, the devices became stretchable with stable device parameters under a compression ratio up to 45%.

In this section, we summarized the high-efficiency flexible and ultra-thin devices based on ITO, AgNWs, and PEDOT:PSS, respectively. Nowadays, outstanding efficiencies and mechanical flexibility are demonstrated in flexible OSCs with different device structures (e.g., conventional and inverted devices, single and tandem layer devices) and various organic photovoltaic materials (e.g., fullerene and nonfullerene materials, binary and ternary blends). These results highlight the great potential of OSCs in bioelectronic applications. However, the long-term stability of the devices is still a big challenge for the OSC community, which should be considered in the future development of flexible devices.

4 OSCs in biomedical devices

In this section, we will discuss several cases of OSC's applications in implantable biomedical devices and sensors. As one of the power generation devices, OSC devices have been combined with additional components in the self-powered bioelectronic devices. As displayed in Fig. 7, Zhang et al. developed an integrated system consisting of a biocompatible OSC device

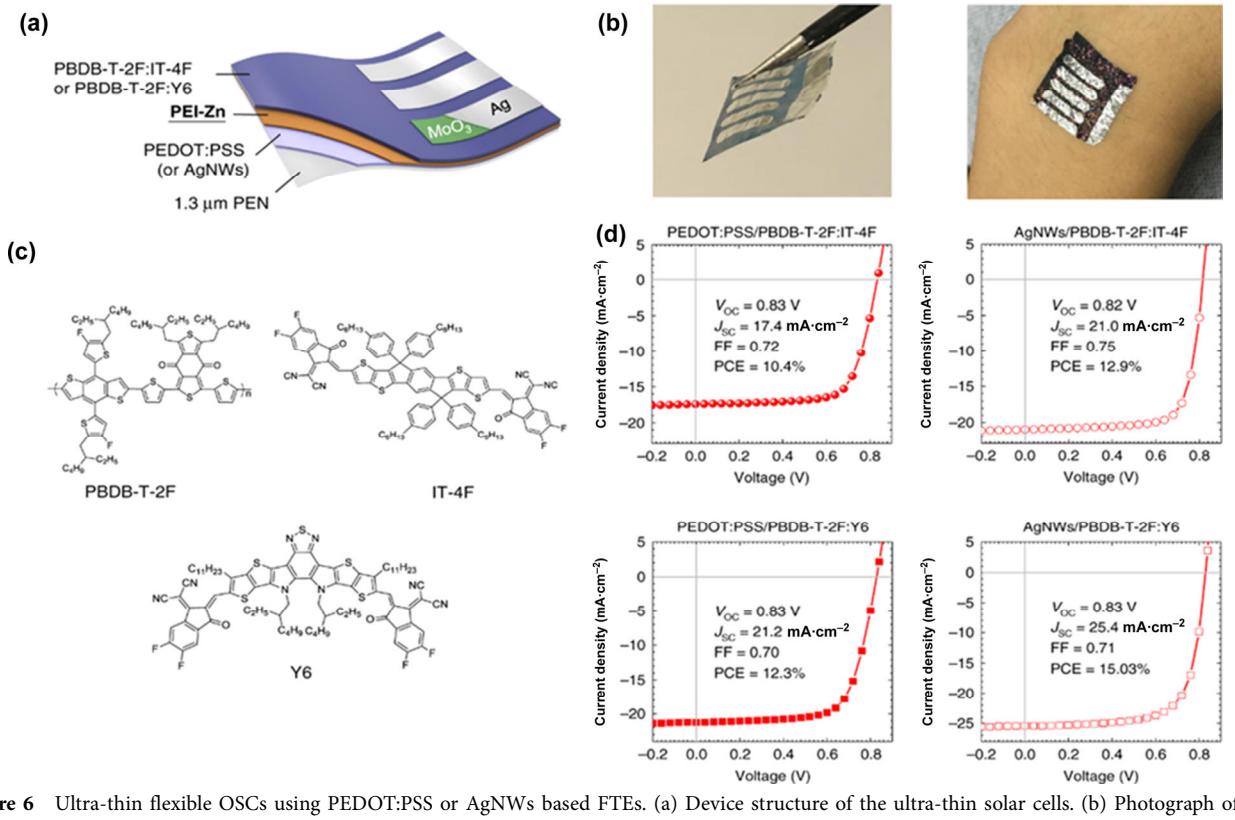

Figure 6 Ultra-thin flexible OSCs using PEDOT:PSS or AgNWs based FTEs. (a) Device structure of the ultra-thin solar cells. (b) Photograph of the fabricated ultrathin device (left) and photograph of the device attached on the wrist (right). (c) Chemical structures of the active layer materials. (d) *J*–*V* curves of the ultrathin devices with PEDOT:PSS or AgNWs as the transparent electrodes. Reproduced with permission from Ref. [24], © Qin F., et al. 2020.

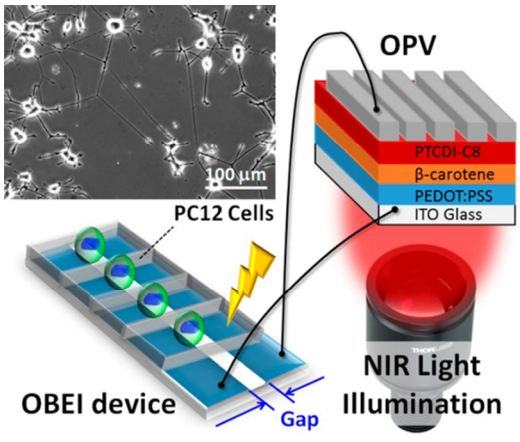

Figure 7 Schematic representation of an OSC/OBEI integrated system for exerting an ES effect on PC12 cells. Reproduced with permission from Ref. [113], © American Chemical Society 2016.

and an organic bioelectronic interface (OBEI) electrode, which is capable of providing electrical stimulation for PC12 cell differentiation and neurite outgrowth [113]. Considering the high-transparency of biological tissues in the near-infrared region, the OSC devices based on β-carotene/PTCDI-C8 and P3HT/PCBM were tested under the near-infrared light illumination, which can generate different V_{oc} of 0.11 and 0.49 V, respectively. By further adjusting the electrode gaps of the OBEI devices, tunable electrical fields in the range of 220–980 mV·mm^{-1} were achievable for the OSC/OBEI integrated devices. The integrated power-delivery bioelectronic devices can promote obvious neurite outgrowth and manipulate the polarity of differentiated PC12 cells. The results indicate that adopting OSC devices as the power source device to design next-generation implantable bioelectronics is a viable approach.

The continuous development of OSCs, including the high-efficiency organic photovoltaic materials, flexible devices with robust mechanical behaviors, and long-term device stability, make them more suitable for usage in bioelectronics. As discussed above, Someya et al. demonstrated ultra-thin, high-efficiency flexible OSCs with excellent mechanical characteristics and extraordinary stability by double-sided polymer passivation. Recently, they conducted a high-throughput room-temperature molding process to form nano-grating morphology on the ZnO electron transporting layer and fabricated ultra-thin flexible OSCs that exhibited a high power-per-weight value of 11.46 W·g^{-1} [44]. Figure 8 shows that the devices can be wrapped over a spatula rod and pulled by tweezers, indicating that the devices can accommodate large mechanical deformations, which is critical for adhesion to dynamic and complex three-dimensional biological tissues and skin. The OSC device was then integrated with an organic electrochemical transistor (OECT) to realize a self-powered flexible biosensor. A conformal self-powered cardiac sensor was demonstrated as shown in Fig. 8. Clear electrocardiogram signals with an SNR of 25.9 dB were recorded with the sensor under LED light illumination because of its good skin conformability. Furthermore, a maximum SNR of 40.02 dB was achieved when the device was attached to the surface of a rat heart. These results highlight the possibility

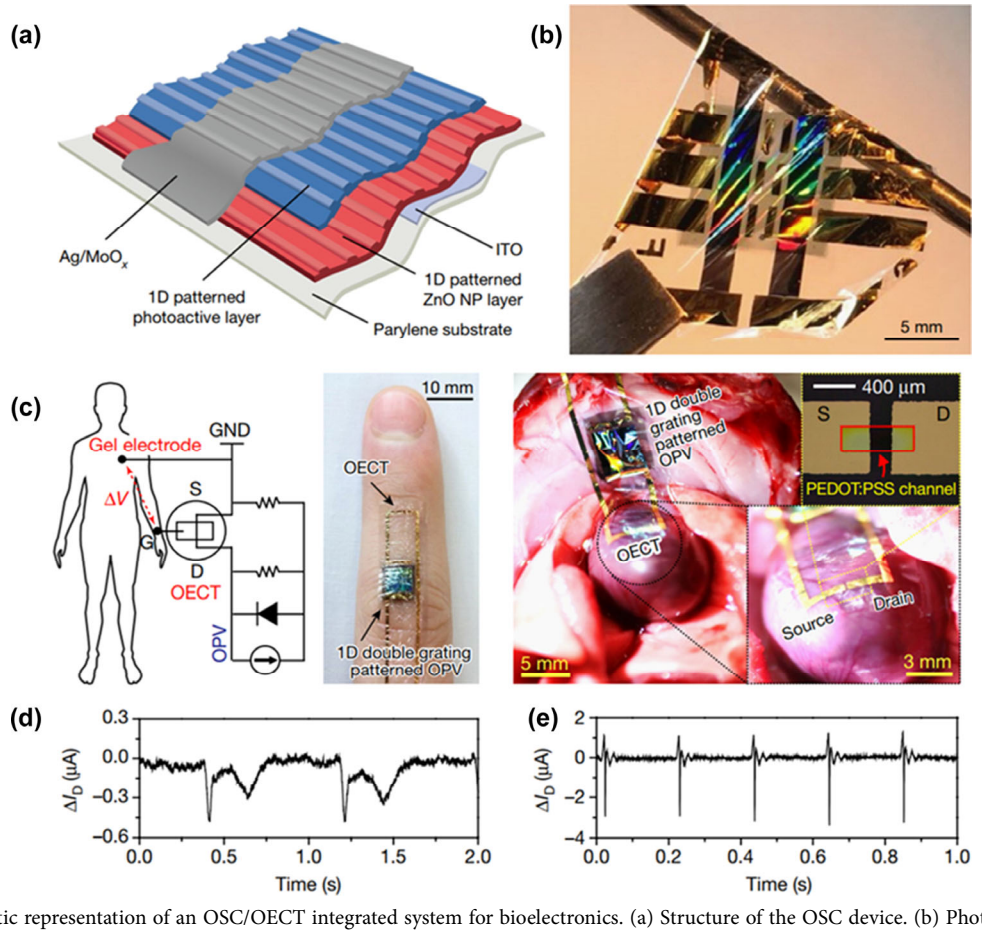

Figure 8 Schematic representation of an OSC/OECT integrated system for bioelectronics. (a) Structure of the OSC device. (b) Photograph of the OSC device wrapped over a spatula rod and pulled by tweezers, after delamination from the supporting glass substrate. (c) Wiring diagram for cardiac signal recording and photograph of the self-powered integrated electronic device attached to a finger or to the heart of a rat, respectively. (d) Measured output current from the recorded cardiac signal trace, under light illumination. (e) Measured output current from the ECG trace, under light illumination. Reproduced with permission from Ref. [44], © Springer Nature Limited 2018.

of accurate and precise acquisition of biological signals by combining the ultra-flexible OSCs as the power source with other functional electronic devices.

A self-powered pressure sensor which consists of a flexible OSC underlying a piezo-transmittance microporous elastomer (PTME) was successfully fabricated for sensing the human finger motions (Fig. 9) [114]. The flexible OSC was fabricated on the commercial ITO/PET substrate using PTB7-Th:$PC_{71}BM$ as the active layer. The intensity of the light transmitted through the PTME increases with the increasing applied pressure, which will affect the current output of the underlying OSC. Recording the current output of OSC device can show the detected applied pressure on the PTME. As a result, the integrated devices exhibited a high sensitivity of 0.101/kPa with a linear behavior. Besides, the sensor showed good mechanical stability and bending insensitive properties, which meet the demands of bioelectronics. Taking advantage of these properties, the pressure sensor was used for finger motion sensing. Figure 9(c) shows that the flexion and extension angles of fingers affect the output current due to the pressure change on the PTME. This work offers a new method to design flexible pressure sensors based on OSCs for bioelectronic devices.

Apart from these aforementioned examples (Table 1), however, OSCs have been fairly less explored or implemented in the biomedical field despite already achieving high efficiency and flexibility. Designing and fabricating bioelectronics powered by the high-efficiency and flexible OSCs still requires greater effort in the near future.

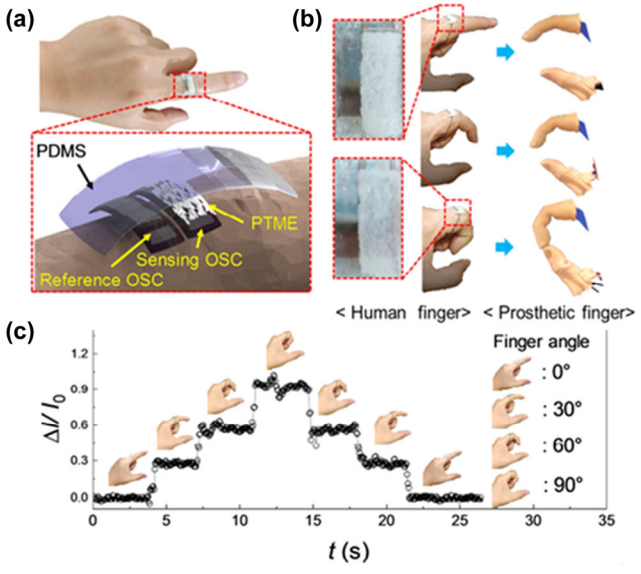

Figure 9 Schematic representation of an OSC/PTME integrated system for bioelectronics. (a) Photograph of a finger with the finger motion sensor on the finger based on the integrated system. (b) Photograph of controlling the prosthetic robot finger using the sensor on the human finger. (c) The sensor response over the finger angle of 0°–90°. Reproduced with permission from Ref. [114], © Elsevier Ltd. 2020.

5 Outlook

In this mini-review, we discussed the rapid development of high-performance organic photovoltaic materials, flexible OSC devices, and the applications of OSCs in biomedical devices. It is encouraging that high PCEs of > 18%, > 16%, and > 15% have been realized in the rigid, flexible, and ultra-thin flexible OSCs, respectively, which can be attributed to the continuous development of novel photovoltaic materials and device engineering. In addition, thin devices can be made stretchable when attached on the pre-strain elastomers, which showed stable performance under stretching and compression.

These attractive merits of OSCs pave the way to develop self-powered bioelectronics that can be integrated on or under the surface of biological tissues. The existing studies have demonstrated their promising potentials in biomedical devices, and the future of such applications can be expected. To further meet the demands of the emerging biomedical devices, improving the OSC's overall efficiency, long-term stability especially in biological environment is still urgent and necessary. One important factor related to improving the efficiency is that the light dosage to human skin and tissues should be maintained below the tissue optical safety threshold. Then, the shined light can be safely absorbed by the human tissues and water. The absorption of light by tissues at the tissue transparent window (700–970 nm) is relatively low. Therefore, the flexible OSCs are required to possess sufficient PCEs at those specific wavelengths to provide the required power. Flexible OSCs constructed from novel organic photovoltaic materials that can absorb near infrared (NIR) light hold promise for biomedical applications. Besides the long-term stability, the flexible OSCs must conform to the target surface to avoid mechanical damage to the human skin or tissues. Additionally, studies of the biocompatibility, dissolvability, or retrievability of the flexible OSCs may be needed to realize long-term biomedical devices.

Apart from the power-generation OSC units, integrating OSCs with various biomedical functionalities including different types of physical and biochemical sensors, drug delivery, and nongenetic optical stimulation can shed light on their future novel bioelectronics applications. We foresee increased utilization of OSCs in creating novel biomedical devices in the near future.

Acknowledgements

C. Y. would like to acknowledge the funding support by the National Institute of Health (R21EB026175, 1R21EB030257-01) and the Office of Naval Research (N00014-18-1-2338) under the Young Investigator Program.

Table 1 A brief summary of representative applications of organic solar cells in biomedical devices

Integrated devices	OSCs					Functionality	Ref.
	Active layer	V_{oc} (V)	J_{sc} (mA·cm^{-2})	FF (%)	PCE (%)		
OSC/OBEI	P3HT:PCBM	0.59	9.66	0.64	3.68	Cell growth; Cell differentiation	[113]
OSC/OECT	PTB7-Th:PCBM	0.785	19.17	69.7	10.49	Sensor; Cardiac signal recording	[44]
OSC/PTME	PTB7-Th:PCBM	—	—	—	—	Pressure sensor; Motion monitoring	[114]

References

[1] Service, R. F. Outlook brightens for plastic solar cells. *Science* **2011**, *332*, 293.

[2] Yu, G.; Gao, J.; Hummelen, J. C.; Wudl, F.; Heeger, A. J. Polymer photovoltaic cells: Enhanced efficiencies via a network of internal donor-acceptor heterojunctions. *Science* **1995**, *270*, 1789–1791.

[3] Proctor, C. M.; Kuik, M.; Nguyen, T. Q. Charge carrier recombination in organic solar cells. *Prog. Polym. Sci.* **2013**, *38*, 1941–1960.

[4] Deibel, C.; Dyakonov, V. Polymer–fullerene bulk heterojunction solar cells. *Rep. Prog. Phys.* **2010**, *73*, 096401.

[5] Dou, L. T.; You, J. B.; Hong, Z. R.; Xu, Z.; Li, G.; Street, R. A.; Yang, Y. 25th anniversary article: A decade of organic/polymeric photovoltaic research. *Adv. Mater.* **2013**, *25*, 6642–6671.

[6] Heeger, A. J. 25th anniversary article: Bulk heterojunction solar cells: Understanding the mechanism of operation. *Adv. Mater.* **2014**, *26*, 10–28.

[7] Lu, L. Y.; Zheng, T. Y.; Wu, Q. H.; Schneider, A. M.; Zhao, D. L.; Yu, L. P. Recent advances in bulk heterojunction polymer solar cells. *Chem. Rev.* **2015**, *115*, 12666–12731.

[8] Gurney, R. S.; Lidzey, D. G.; Wang, T. A review of non-fullerene polymer solar cells: From device physics to morphology control. *Rep. Prog. Phys.* **2019**, *82*, 036601.

[9] Cui, Y.; Yao, H. F.; Zhang, J. Q.; Xian, K. H.; Zhang, T.; Hong, L.; Wang, Y. M.; Xu, Y.; Ma, K. Q.; An, C. B. et al. Single-junction organic photovoltaic cells with approaching 18% efficiency. *Adv. Mater.* **2020**, *32*, 1908205.

[10] Liu, Q. S.; Jiang, Y. F.; Jin, K.; Qin, J. Q.; Xu, J. G.; Li, W. T.; Xiong, J.; Liu, J. F.; Xiao, Z.; Sun, K. et al. 18% Efficiency organic solar cells. *Sci. Bull.* **2020**, *65*, 272–275.

[11] Lin, Y. B.; Firdaus, Y.; Isikgor, F. H.; Nugraha, M. I.; Yengel, E.; Harrison, G. T.; Hallani, R.; El-Labban, A.; Faber, H.; Ma, C. et al. Self-assembled monolayer enables hole transport layer-free organic solar cells with 18% efficiency and improved operational stability. *ACS Energy Lett.* **2020**, *5*, 2935–2944.

[12] Meng, L. X.; Zhang, Y. M.; Wan, X. J.; Li, C. X.; Zhang, X.; Wang, Y. B.; Ke, X.; Xiao, Z.; Ding, L. M.; Xia, R. X. et al. Organic and solution-processed tandem solar cells with 17.3% efficiency. *Science* **2018**, *361*, 1094–1098.

[13] Zhang, G. Y.; Zhao, J. B.; Chow, P. C. Y.; Jiang, K.; Zhang, J. Q.; Zhu, Z. L.; Zhang, J.; Huang, F.; Yan, H. Nonfullerene acceptor molecules for bulk heterojunction organic solar cells. *Chem. Rev.* **2018**, *118*, 3447–3507.

[14] Yan, C. Q.; Barlow, S.; Wang, Z. H.; Yan, H.; Jen, A. K. Y.; Marder, S. R.; Zhan, X. W. Non-fullerene acceptors for organic solar cells. *Nat. Rev. Mater.* **2018**, *3*, 18003.

[15] Wadsworth, A.; Moser, M.; Marks, A.; Little, M. S.; Gasparini, N.; Brabec, C. J.; Baran, D.; McCulloch, I. Critical review of the molecular design progress in non-fullerene electron acceptors towards commercially viable organic solar cells. *Chem. Soc. Rev.* **2019**, *48*, 1596–1625.

[16] Zhang, X.; Ding, Y. Q.; Feng, H. R.; Gao, H. H.; Ke, X.; Zhang, H. T.; Li, C. X.; Wan, X. J.; Chen, Y. S. Side chain engineering investigation of non-fullerene acceptors for photovoltaic device with efficiency over 15%. *Sci. China Chem.* **2020**, *63*, 1799–1806.

[17] Inganäs, O. Organic photovoltaics over three decades. *Adv. Mater.* **2018**, *30*, 1800388.

[18] Li, S. X.; Zhan, L. L.; Jin, Y. Z.; Zhou, G. Q.; Lau, T. K.; Qin, R.; Shi, M. M.; Li, C. Z.; Zhu, H. M.; Lu, X. H. et al. Asymmetric electron acceptors for high-efficiency and low-energy-loss organic photovoltaics. *Adv. Mater.* **2020**, *32*, 2001160.

[19] Hou, J. H.; Inganäs, O.; Friend, R. H.; Gao, F. Organic solar cells based on non-fullerene acceptors. *Nat. Mater.* **2018**, *17*, 119–128.

[20] Xu, G. Y.; Li, Y. W. Metal-microstructure based flexible transparent electrodes and their applications in electronic devices. *Nano Select* **2020**, *1*, 169–182.

[21] Qin, J. Q.; Lan, L. K.; Chen, S. S.; Huang, F. N.; Shi, H. R.; Chen, W. J.; Xia, H. B.; Sun, K.; Yang, C. Recent progress in flexible and stretchable organic solar cells. *Adv. Funct. Mater.* **2020**, *30*, 2002529.

[22] Sun, Y. N.; Chang, M. J.; Meng, L. X.; Wan, X. J.; Gao, H. H.; Zhang, Y. M.; Zhao, K.; Sun, Z. H.; Li, C. X.; Liu, S. R. et al. Flexible organic photovoltaics based on water-processed silver nanowire electrodes. *Nat. Electron.* **2019**, *2*, 513–520.

[23] Qu, T. Y.; Zuo, L. J.; Chen, J. D.; Shi, X. L.; Zhang, T.; Li, L.; Shen, K. C.; Ren, H.; Wang, S.; Xie, F. M. et al. Biomimetic electrodes for flexible organic solar cells with efficiencies over 16%. *Adv. Opt. Mater.* **2020**, *8*, 2000669.

[24] Qin, F.; Wang, W.; Sun, L. L.; Jiang, X. S.; Hu, L.; Xiong, S. X.; Liu, T. F.; Dong, X. Y.; Li, J.; Jiang, Y. Y. et al. Robust metal ion-chelated polymer interfacial layer for ultraflexible non-fullerene organic solar cells. *Nat. Commun.* **2020**, *11*, 4508.

[25] Chen, X. B.; Xu, G. Y.; Zeng, G.; Gu, H. W.; Chen, H. Y.; Xu, H. T.; Yao, H. F.; Li, Y. W.; Hou, J. H.; Li, Y. F. Realizing ultrahigh mechanical flexibility and >15% efficiency of flexible organic solar cells via a "welding" flexible transparent electrode. *Adv. Mater.* **2020**, *32*, 1908478.

[26] Koo, D.; Jung, S.; Seo, J.; Jeong, G.; Choi, Y.; Lee, J.; Lee, S. M.; Cho, Y.; Jeong, M.; Lee, J. et al. Flexible organic solar cells over 15% efficiency with polyimide-integrated graphene electrodes. *Joule* **2020**, *4*, 1021–1034.

[27] Sullivan, P.; Schumann, S.; Da Campo, R.; Howells, T.; Duraud, A.; Shipman, M.; Hatton, R. A.; Jones, T. S. Ultra-high voltage multijunction organic solar cells for low-power electronic applications. *Adv. Energy Mater.* **2013**, *3*, 239–244.

[28] Schmidt, D.; Hager, M. D.; Schubert, U. S. Photo-rechargeable electric energy storage systems. *Adv. Energy Mater.* **2016**, *6*, 1500369.

[29] Zeng, Q.; Lai, Y. Q.; Jiang, L. X.; Liu, F. Y.; Hao, X. J.; Wang, L. Z.; Green, M. A. Integrated photorechargeable energy storage system: Next-generation power source driving the future. *Adv. Energy Mater.* **2020**, *10*, 1903930.

[30] Liu, R. Y.; Takakuwa, M.; Li, A. L.; Inoue, D.; Hashizume, D.; Yu, K.; Umezu, S.; Fukuda, K.; Someya, T. An efficient ultra-flexible photo-charging system integrating organic photovoltaics and supercapacitors. *Adv. Energy Mater.* **2020**, *10*, 2000523.

[31] Yao, L.; Rahmanudin, A.; Guijarro, N.; Sivula, K. Organic semiconductor based devices for solar water splitting. *Adv. Energy Mater.* **2018**, *8*, 1802585.

[32] Ghobadi, A.; Ulusoy Ghobadi, T. G.; Karadas, F.; Ozbay, E. Semiconductor thin film based metasurfaces and metamaterials for photovoltaic and photoelectrochemical water splitting applications. *Adv. Opt. Mater.* **2019**, *7*, 1900028.

[33] Wang, D. G.; Hu, J.; Sherman, B. D.; Sheridan, M. V.; Yan, L.; Dares, C. J.; Zhu, Y.; Li, F.; Huang, Q.; You, W. et al. A molecular tandem cell for efficient solar water splitting. *Proc. Natl. Acad. Sci. USA* **2020**, *117*, 13256–13260.

[34] Chen, F. C. Emerging organic and organic/inorganic hybrid photovoltaic devices for specialty applications: Low-level-lighting energy conversion and biomedical treatment. *Adv. Opt. Mater.* **2019**, *7*, 1800662.

[35] Yu, K.; Rich, S.; Lee, S.; Fukuda, K.; Yokota, T.; Someya, T. Organic photovoltaics: Toward self-powered wearable electronics. *Proc. IEEE* **2019**, *107*, 2137–2154.

[36] Hashemi, S. A.; Ramakrishna, S.; Aberle, A. G. Recent progress in flexible–wearable solar cells for self-powered electronic devices. *Energy Environ. Sci.* **2020**, *13*, 685–743.

[37] Mühl, S.; Beyer, B. Bio-organic electronics—overview and prospects for the future. *Electronics* **2014**, *3*, 444–461.

[38] Yokota, T.; Zalar, P.; Kaltenbrunner, M.; Jinno, H.; Matsuhisa, N.; Kitanosako, H.; Tachibana, Y.; Yukita, W.; Koizumi, M.; Someya, T. Ultraflexible organic photonic skin. *Sci. Adv.* **2016**, *2*, e1501856.

[39] Chen, Z. Y.; Obaid, S. N.; Lu, L. Y. Recent advances in organic optoelectronic devices for biomedical applications. *Opt. Mater. Express* **2019**, *9*, 3843–3856.

[40] Ershad, F.; Sim, K.; Thukral, A.; Zhang, Y. S.; Yu, C. J. Invited Article: Emerging soft bioelectronics for cardiac health diagnosis and treatment. *APL Mater.* **2019**, *7*, 031301.

[41] Wangatia, L. M.; Yang, S. Y.; Zabihi, F.; Zhu, M. F.; Ramakrishna, S. Biomedical electronics powered by solar cells. *Curr. Opin. Biomed. Eng.* **2020**, *13*, 25–31.

[42] Lee, G. H.; Moon, H.; Kim, H.; Lee, G. H.; Kwon, W.; Yoo, S.; Myung, D.; Yun, S. H.; Bao, Z. N.; Hahn, S. K. Multifunctional materials for implantable and wearable photonic healthcare devices. *Nat. Rev. Mater.* **2020**, *5*, 149–165.

[43] Rao, Z. L.; Ershad, F.; Almasri, A.; Gonzalez, L.; Wu, X. Y.; Yu, C. J. Soft electronics for the skin: From health monitors to human–machine interfaces. *Adv. Mater. Technol.* **2020**, *5*, 2000233.
[44] Park, S.; Heo, S. W.; Lee, W.; Inoue, D.; Jiang, Z.; Yu, K.; Jinno, H.; Hashizume, D.; Sekino, M.; Yokota, T. et al. Self-powered ultra-flexible electronics via nano-grating-patterned organic photovoltaics. *Nature* **2018**, *561*, 516–521.
[45] Clarke, T. M.; Durrant, J. R. Charge photogeneration in organic solar cells. *Chem. Rev.* **2010**, *110*, 6736–6767.
[46] Pfannmöller, M.; Kowalsky, W.; Schröder, R. R. Visualizing physical, electronic, and optical properties of organic photovoltaic cells. *Energy Environ. Sci.* **2013**, *6*, 2871–2891.
[47] Tong, Y.; Xiao, Z.; Du, X. Y.; Zuo, C. T.; Li, Y. L.; Lv, M. L.; Yuan, Y. B.; Yi, C. Y.; Hao, F.; Hua, Y. et al. Progress of the key materials for organic solar cells. *Sci. China Chem.* **2020**, *63*, 758–765.
[48] Dang, M. T.; Hirsch, L.; Wantz, G.; Wuest, J. D. Controlling the morphology and performance of bulk heterojunctions in solar cells. Lessons learned from the benchmark poly(3-hexylthiophene): [6,6]-phenyl-C_{61}-butyric acid methyl ester system. *Chem. Rev.* **2013**, *113*, 3734–3765.
[49] Zhang, L.; Colella, N. S.; Cherniawski, B. P.; Mannsfeld, S. C. B.; Briseno, A. L. Oligothiophene semiconductors: Synthesis, characterization, and applications for organic devices. *ACS Appl. Mater. Interfaces* **2014**, *6*, 5327–5343.
[50] Ye, L.; Zhang, S. Q.; Huo, L. J.; Zhang, M. J.; Hou, J. H. Molecular design toward highly efficient photovoltaic polymers based on two-dimensional conjugated benzodithiophene. *Acc. Chem. Res.* **2014**, *47*, 1595–1603.
[51] Lu, L. Y.; Yu, L. P. Understanding low bandgap polymer PTB7 and optimizing polymer solar cells based on it. *Adv. Mater.* **2014**, *26*, 4413–4430.
[52] Chen, Y. S.; Wan, X. J.; Long, G. K. High performance photovoltaic applications using solution-processed small molecules. *Acc. Chem. Res.* **2013**, *46*, 2645–2655.
[53] Kan, B.; Li, M. M.; Zhang, Q.; Liu, F.; Wan, X. J.; Wang, Y. C.; Ni, W.; Long, G. K.; Yang, X.; Feng, H. R. et al. A series of simple oligomer-like small molecules based on oligothiophenes for solution-processed solar cells with high efficiency. *J. Am. Chem. Soc.* **2015**, *137*, 3886–3893.
[54] Coughlin, J. E.; Henson, Z. B.; Welch, G. C.; Bazan, G. C. Design and synthesis of molecular donors for solution-processed high-efficiency organic solar cells. *Acc. Chem. Res.* **2014**, *47*, 257–270.
[55] Li, M. M.; Gao, K.; Wan, X. J.; Zhang, Q.; Kan, B.; Xia, R. X.; Liu, F.; Yang, X.; Feng, H. R.; Ni, W. et al. Solution-processed organic tandem solar cells with power conversion efficiencies >12%. *Nat. Photon.* **2017**, *11*, 85–90.
[56] Kumari, T.; Lee, S. M.; Kang, S. H.; Chen, S. S.; Yang, C. Ternary solar cells with a mixed face-on and edge-on orientation enable an unprecedented efficiency of 12.1%. *Energy Environ. Sci.* **2017**, *10*, 258–265.
[57] Chen, W. Q.; Zhang, Q. C. Recent progress in non-fullerene small molecule acceptors in organic solar cells (OSCs). *J. Mater. Chem. C* **2017**, *5*, 1275–1302.
[58] Li, S. X.; Li, C. Z.; Shi, M. M.; Chen, H. Z. New phase for organic solar cell research: Emergence of Y-series electron acceptors and their perspectives. *ACS Energy Lett.* **2020**, *5*, 1554–1567.
[59] Lin, Y. Z.; Zhan, X. W. Designing efficient non-fullerene acceptors by tailoring extended fused-rings with electron-deficient groups. *Adv. Energy Mater.* **2015**, *5*, 1501063.
[60] Jia, T.; Zhang, J. B.; Zhong, W. K.; Liang, Y. Y.; Zhang, K.; Dong, S.; Ying, L.; Liu, F.; Wang, X. H.; Huang, F. et al. 14.4% efficiency all-polymer solar cell with broad absorption and low energy loss enabled by a novel polymer acceptor. *Nano Energy* **2020**, *72*, 104718.
[61] Yao, H. F.; Wang, J. W.; Xu, Y.; Zhang, S. Q.; Hou, J. H. Recent progress in chlorinated organic photovoltaic materials. *Acc. Chem. Res.* **2020**, *53*, 822–832.
[62] Fu, H. T.; Wang, Z. H.; Sun, Y. M. Polymer donors for high-performance non-fullerene organic solar cells. *Angew. Chem., Int. Ed.* **2019**, *58*, 4442–4453.
[63] Zhao, W. C.; Qian, D. P.; Zhang, S. Q.; Li, S. S.; Inganäs, O.; Gao, F.; Hou, J. H. Fullerene-free polymer solar cells with over 11% efficiency and excellent thermal stability. *Adv. Mater.* **2016**, *28*, 4734–4739.
[64] Zhang, M. J.; Guo, X.; Ma, W.; Ade, H.; Hou, J. H. A large-bandgap conjugated polymer for versatile photovoltaic applications with high performance. *Adv. Mater.* **2015**, *27*, 4655–4660.
[65] Fan, Q. P.; Su, W. Y.; Wang, Y.; Guo, B.; Jiang, Y. F.; Guo, X.; Liu, F.; Russell, T. P.; Zhang, M.; Li, Y. F. Synergistic effect of fluorination on both donor and acceptor materials for high performance non-fullerene polymer solar cells with 13.5% efficiency. *Sci. China Chem.* **2018**, *61*, 531–537.
[66] Yuan, J.; Zhang, Y. Q.; Zhou, L. Y.; Zhang, G. C.; Yip, H. L.; Lau, T. K.; Lu, X. H.; Zhu, C.; Peng, H. J.; Johnson, P. A. et al. Single-junction organic solar cell with over 15% efficiency using fused-ring acceptor with electron-deficient core. *Joule* **2019**, *3*, 1140–1151.
[67] Zhang, M.; Zhu, L.; Zhou, G. Q.; Hao, T. Y.; Qiu, C. Q.; Zhao, Z.; Hu, Q.; Larson, B. W.; Zhu, H. M.; Ma, Z. F. et al. Single-layered organic photovoltaics with double cascading charge transport pathways: 18% effciencies. *Nat. Commun.* **2021**, *12*, 309.
[68] Wei, Q. Y.; Liu, W.; Leclerc, M.; Yuan, J.; Chen, H. G.; Zou, Y. P. A-DA′D-A non-fullerene acceptors for high-performance organic solar cells. *Sci. China Chem.* **2020**, *63*, 1352–1366.
[69] Walker, B.; Kim, C.; Nguyen, T. Q. Small molecule solution-processed bulk heterojunction solar cells. *Chem. Mater.* **2011**, *23*, 470–482.
[70] Mishra, A.; Bäuerle, P. Small molecule organic semiconductors on the move: Promises for future solar energy technology. *Angew. Chem., Int. Ed.* **2012**, *51*, 2020–2067.
[71] Lin, Y. Z.; Zhan, X. W. Oligomer molecules for efficient organic photovoltaics. *Acc. Chem. Res.* **2016**, *49*, 175–183.
[72] Huo, Y.; Zhang, H. L.; Zhan, X. W. Nonfullerene all-small-molecule organic solar cells. *ACS Energy Lett.* **2019**, *4*, 1241–1250.
[73] Liang, N. N.; Meng, D.; Ma, Z. T.; Kan, B.; Meng, X. Y.; Zheng, Z.; Jiang, W.; Li, Y.; Wan, X. J.; Hou, J. H. et al. Triperylene hexaimides based all-small-molecule solar cells with an efficiency over 6% and open circuit voltage of 1.04 V. *Adv. Energy Mater.* **2017**, *7*, 1601664.
[74] Lin, Y. Z.; He, Q.; Zhao, F. W.; Huo, L. J.; Mai, J. Q.; Lu, X. H.; Su, C. J.; Li, T. F.; Wang, J. Y.; Zhu, J. S. et al. A Facile planar fused-ring electron acceptor for as-cast polymer solar cells with 8.71% efficiency. *J. Am. Chem. Soc.* **2016**, *138*, 2973–2976.
[75] Yang, L. Y.; Zhang, S. Q.; He, C.; Zhang, J. Q.; Yao, H. F.; Yang, Y.; Zhang, Y.; Zhao, W. C.; Hou, J. H. New wide band gap donor for efficient fullerene-free all-small-molecule organic solar cells. *J. Am. Chem. Soc.* **2017**, *139*, 1958–1966.
[76] Zhang, H.; Wang, X. H.; Yang, L. Y.; Zhang, S. Q.; Zhang, Y.; He, C.; Ma, W.; Hou, J. H. Improved domain size and purity enables efficient all-small-molecule ternary solar cells. *Adv. Mater.* **2017**, *29*, 1703777.
[77] Guo, J.; Bin, H. J.; Wang, W.; Chen, B. C.; Guo, J.; Sun, R.; Zhang, Z. G.; Jiao, X. C.; Li, Y. F.; Min, J. All-small molecule solar cells based on donor molecule optimization with highly enhanced efficiency and stability. *J. Mater. Chem. A* **2018**, *6*, 15675–15683.
[78] Wang, Y. C.; Wang, Y. B.; Kan, B.; Ke, X.; Wan, X. J.; Li, C. X.; Chen, Y. S. High-performance all-small-molecule solar cells based on a new type of small molecule acceptors with chlorinated end groups. *Adv. Energy Mater.* **2018**, *8*, 1802021.
[79] Chen, H. Y.; Hu, D. Q.; Yang, Q. G.; Gao, J.; Fu, J. H.; Yang, K.; He, H.; Chen, S. S.; Kan, Z. P.; Duan, T. N. et al. All-small-molecule organic solar cells with an ordered liquid crystalline donor. *Joule* **2019**, *3*, 3034–3047.
[80] Qin, J. Z.; An, C. B.; Zhang, J. Q.; Ma, K.; Yang, Y.; Zhang, T.; Li, S.; Xian, K. H.; Cui, Y.; Tang, Y. B. et al. 15.3% efficiency all-small-molecule organic solar cells enabled by symmetric phenyl substitution. *Sci. China Mater.* **2020**, *63*, 1142–1150.
[81] Lee, C.; Lee, S.; Kim, G. U.; Lee, W.; Kim, B. J. Recent advances, design guidelines, and prospects of all-polymer solar cells. *Chem. Rev.* **2019**, *119*, 8028–8086.
[82] Fan, Q. P.; Su, W. Y.; Chen, S. S.; Kim, W. S.; Chen, X. B.; Lee, B.; Liu, T.; Méndez-Romero, U. A.; Ma, R. J.; Yang, T. et al. Mechanically robust all-polymer solar cells from narrow band gap acceptors with hetero-bridging atoms. *Joule* **2020**, *4*, 658–672.
[83] Yan, H.; Chen, Z. H.; Zheng, Y.; Newman, C.; Quinn, J. R.; Dötz, F.; Kastler, M.; Facchetti, A. A high-mobility electron-transporting polymer for printed transistors. *Nature* **2009**, *457*, 679–686.
[84] Fabiano, S.; Chen, Z.; Vahedi, S.; Facchetti, A.; Pignataro, B.; Loi, M. A. Role of photoactive layer morphology in high fill factor

all-polymer bulk heterojunction solar cells. *J. Mater. Chem.* **2011**, *21*, 5891–5896.

[85] Li, Z. J.; Xu, X. F.; Zhang, W.; Meng, X. Y.; Ma, W.; Yartsev, A.; Inganäs, O.; Andersson, M. R.; Janssen, R. A. J.; Wang, E. G. High performance all-polymer solar cells by synergistic effects of fine-tuned crystallinity and solvent annealing. *J. Am. Chem. Soc.* **2016**, *138*, 10935–10944.

[86] Fan, B. B.; Ying, L.; Zhu, P.; Pan, F. L.; Liu, F.; Chen, J. W.; Huang, F.; Cao, Y. All-polymer solar cells based on a conjugated polymer containing siloxane-functionalized side chains with efficiency over 10%. *Adv. Mater.* **2017**, *29*, 1703906.

[87] Gao, L.; Zhang, Z. G.; Xue, L. W.; Min, J.; Zhang, J. Q.; Wei, Z. X.; Li, Y. F. All-polymer solar cells based on absorption-complementary polymer donor and acceptor with high power conversion efficiency of 8.27%. *Adv. Mater.* **2016**, *28*, 1884–1890.

[88] Zhang, Z. G.; Yang, Y. K.; Yao, J.; Xue, L. W.; Chen, S. S.; Li, X. J.; Morrison, W.; Yang, C.; Li, Y. F. Constructing a strongly absorbing low-bandgap polymer acceptor for high-performance all-polymer solar cells. *Angew. Chem., Int. Ed.* **2017**, *56*, 13503–13507.

[89] Wu, Q.; Wang, W.; Wang, T.; Sun, R.; Guo, J.; Wu, Y.; Jiao, X. C.; Brabec, C. J.; Li, Y. F.; Min, J. High-performance all-polymer solar cells with only 0.47 eV energy loss. *Sci. China Chem.* **2020**, *63*, 1449–1460.

[90] Zhang, Z. J.; Miao, J. H.; Ding, Z. C.; Kan, B.; Lin, B. J.; Wan, X. J.; Ma, W.; Chen, Y. S.; Long, X. J.; Dou, C. D. et al. Efficient and thermally stable organic solar cells based on small molecule donor and polymer acceptor. *Nat. Commun.* **2019**, *10*, 3271.

[91] Lu, S. D.; Sun, Y.; Ren, K. K.; Liu, K.; Wang, Z. J.; Qu, S. C. Recent development in ITO-free flexible polymer solar cells. *Polymers* **2018**, *10*, 5.

[92] Fukuda, K.; Yu, K.; Someya, T. The future of flexible organic solar cells. *Adv. Energy Mater.* **2020**, *10*, 2000765.

[93] Chen, J. Y.; Zhou, W. X.; Chen, J.; Fan, Y.; Zhang, Z. Q.; Huang, Z. D.; Feng, X. M.; Mi, B. X.; Ma, Y. W.; Huang, W. Solution-processed copper nanowire flexible transparent electrodes with PEDOT: PSS as binder, protector and oxide-layer scavenger for polymer solar cells. *Nano Res.* **2015**, *8*, 1017–1025.

[94] Zhai, H. T.; Li, Y.; Chen, L. W.; Wang, X.; Shi, L. J.; Wang, R. R.; Sun, J. Semi-transparent polymer solar cells with all-copper nanowire electrodes. *Nano Res.* **2018**, *11*, 1956–1966.

[95] Xiong, S. X.; Hu, L.; Hu, L.; Sun, L. L.; Qin, F.; Liu, X. J.; Fahlman, M.; Zhou, Y. H. 12.5% flexible nonfullerene solar cells by passivating the chemical interaction between the active layer and polymer interfacial layer. *Adv. Mater.* **2019**, *31*, 1806616.

[96] Jinno, H.; Fukuda, K.; Xu, X. M.; Park, S.; Suzuki, Y.; Koizumi, M.; Yokota, T.; Osaka, I.; Takimiya, K.; Someya, T. Stretchable and waterproof elastomer-coated organic photovoltaics for washable electronic textile applications. *Nat. Energy* **2017**, *2*, 780–785.

[97] Xu, X. M.; Fukuda, K.; Karki, A.; Park, S.; Kimura, H.; Jinno, H.; Watanabe, N.; Yamamoto, S.; Shimomura, S.; Kitazawa, D. et al. Thermally stable, highly efficient, ultraflexible organic photovoltaics. *Proc. Natl. Acad. Sci. USA* **2018**, *115*, 4589–4594.

[98] Morales-Masis, M.; De Wolf, S.; Woods-Robinson, R.; Ager, J. W.; Ballif, C. Transparent electrodes for efficient optoelectronics. *Adv. Electron. Mater.* **2017**, *3*, 1600529.

[99] Basarir, F.; Irani, F. S.; Kosemen, A.; Camic, B. T.; Oytun, F.; Tunaboylu, B.; Shin, H. J.; Nam, K. Y.; Choi, H. Recent progresses on solution-processed silver nanowire based transparent conducting electrodes for organic solar cells. *Mater. Today Chem.* **2017**, *3*, 60–72.

[100] Park, H.; Brown, P. R.; Bulović, V.; Kong, J. Graphene as transparent conducting electrodes in organic photovoltaics: Studies in graphene morphology, hole transporting layers, and counter electrodes. *Nano Lett.* **2012**, *12*, 133–140.

[101] Lee, H. B.; Jin, W. Y.; Ovhal, M. M.; Kumar, N.; Kang, J. W. Flexible transparent conducting electrodes based on metal meshes for organic optoelectronic device applications: A review. *J. Mater. Chem. C* **2019**, *7*, 1087–1110.

[102] Lee, J. Y.; Connor, S. T.; Cui, Y.; Peumans, P. Solution-processed metal nanowire mesh transparent electrodes. *Nano Lett.* **2008**, *8*, 689–692.

[103] Yang, L. Q.; Zhang, T.; Zhou, H. X.; Price, S. C.; Wiley, B. J.; You, W. Solution-processed flexible polymer solar cells with silver nanowire electrodes. *ACS Appl. Mater. Interfaces* **2011**, *3*, 4075–4084.

[104] Fan, X.; Nie, W. Y.; Tsai, H.; Wang, N. X.; Huang, H. H.; Cheng, Y. J.; Wen, R. J.; Ma, L. J.; Yan, F.; Xia, Y. G. PEDOT: PSS for flexible and stretchable electronics: Modifications, strategies, and applications. *Adv. Sci.* **2019**, *6*, 1900813.

[105] Kim, S. M.; Kim, C. H.; Kim, Y.; Kim, N.; Lee, W. J.; Lee, E. H.; Kim, D.; Park, S.; Lee, K.; Rivnay, J. et al. Influence of PEDOT: PSS crystallinity and composition on electrochemical transistor performance and long-term stability. *Nat. Commun.* **2018**, *9*, 3858.

[106] Sun, K.; Zhang, S. P.; Li, P. C.; Xia, Y. J.; Zhang, X.; Du, D. H.; Isikgor, F. H.; Ouyang, J. Y. Review on application of PEDOTs and PEDOT: PSS in energy conversion and storage devices. *J. Mater. Sci. Mater. Electron.* **2015**, *26*, 4438–4462.

[107] Jiang, Y. Y.; Liu, T. F.; Zhou, Y. H. Recent advances of synthesis, properties, film fabrication methods, modifications of poly(3,4-ethylenedioxythiophene), and applications in solution-processed photovoltaics. *Adv. Funct. Mater.* **2020** *30*, 2006213.

[108] Xia, Y. J.; Dai, S. Y. Review on applications of PEDOTs and PEDOT:PSS in perovskite solar cells. *J. Mater. Sci. Mater. Electron.* **2020**, DOI: 10.1007/s10854-020-03473-w.

[109] Song, W.; Fan, X.; Xu, B. G.; Yan, F.; Cui, H. Q.; Wei, Q.; Peng, R. X.; Hong, L.; Huang, J. M.; Ge, Z. Y. All-solution-processed metal-oxide-free flexible organic solar cells with over 10% efficiency. *Adv. Mater.* **2018**, *30*, 1800075.

[110] Yan, T. T.; Song, W.; Huang, J. M.; Peng, R. X.; Huang, L. K.; Ge, Z. Y. 16.67% Rigid and 14.06% flexible organic solar cells enabled by ternary heterojunction strategy. *Adv. Mater.* **2019**, *31*, 1902210.

[111] Wong, K. W.; Yip, H. L.; Luo, Y.; Wong, K. Y.; Lau, W. M.; Low, K. H.; Chow, H. F.; Gao, Z. Q.; Yeung, W. L.; Chang, C. C. Blocking reactions between indium-tin oxide and poly (3,4-ethylene dioxythiophene): Poly(styrene sulphonate) with a self-assembly monolayer. *Appl. Phys. Lett.* **2002**, *80*, 2788–2790.

[112] Jørgensen, M.; Norrman, K.; Krebs, F. C. Stability/degradation of polymer solar cells. *Sol. Energy Mater. Sol. Cells* **2008**, *92*, 686–714.

[113] Hsiao, Y. S.; Liao, Y. H.; Chen, H. L.; Chen, P. L.; Chen, F. C. Organic photovoltaics and bioelectrodes providing electrical stimulation for PC12 cell differentiation and neurite outgrowth. *ACS Appl. Mater. Interfaces* **2016**, *8*, 9275–9284.

[114] Choi, J.; Kwon, D.; Kim, B.; Kang, K.; Gu, J. M.; Jo, J.; Na, K.; Ahn, J.; Del Orbe, D.; Kim, K. et al. Wearable self-powered pressure sensor by integration of piezo-transmittance microporous elastomer with organic solar cell. *Nano Energy* **2020**, *74*, 104749.